Osteoporos Int (2002) 13:6–17


**Osteoporosis International**

*Original Article*

# In Vivo Assessment of Architecture and Micro-Finite Element Analysis Derived Indices of Mechanical Properties of Trabecular Bone in the Radius

D. C. Newitt[1], S. Majumdar[1], B. van Rietbergen[2], G. von Ingersleben[3*], S. T. Harris[4], H. K. Genant[4], C. Chesnut[3], P. Garnero[5*] and B. MacDonald[6]

[1]Magnetic Resonance Science Center, University of California, San Francisco, USA; [2]University of Eindhoven, Eindhoven, The Netherlands; [3]University of Washington, Seattle, USA; [4]Osteoporosis and Arthritis Research Group, University of California, San Francisco, USA; [5]INSERM, Unit 403, Lyon, France; and [6]Smith Kline Beecham Pharmaceuticals, USA

**Abstract.** Measurement of microstructural parameters of trabecular bone noninvasively in vivo is possible with high-resolution magnetic resonance (MR) imaging. These measurements may prove useful in the determination of bone strength and fracture risk, but must be related to other measures of bone properties. In this study in vivo MR imaging was used to derive trabecular bone structure measures and combined with micro-finite element analysis ($\mu$FE) to determine the effects of trabecular bone microarchitecture on bone mechanical properties in the distal radius. The subjects were studied in two groups: (I) postmenopausal women with normal bone mineral density (BMD) ($n = 22$, mean age 58 $\pm$ 7 years) and (II) postmenopausal women with spine or femur BMD $-1$ SD to $-2.5$ SD below young normal ($n = 37$, mean age 62 $\pm$ 11 years). MR images of the distal radius were obtained at 1.5 T, and measures such as apparent trabecular bone volume fraction (App BV/TV), spacing, number and thickness (App TbSp, TbN, TbTh) were derived in regions of interest extending from the joint line to the radial shaft. The high-resolution images were also used in a micro-finite element model to derive the directional Young's moduli (E1, E2 and E3), shear moduli (G12, G23 and G13) and anisotropy ratios such as E1/E3. BMD at the distal radius, lumbar spine and hip were assessed using dual-energy X-ray absorptiometry (DXA). Bone formation was assessed by serum osteocalcin and bone resorption by serum type I collagen C-terminal telopeptide breakdown products (serum CTX) and urinary CTX biochemical markers. The trabecular architecture displayed considerable anisotropy. Measures of BMD such as the ultradistal radial BMD were lower in the osteopenic group ($p<0.01$). Biochemical markers between the two groups were comparable in value and showed no significant difference between the two groups. App BV/TV, TbTh and TbN were higher, and App TbSp lower, in the normal group than the osteopenic group. All three directional measures of elastic and shear moduli were lower in the osteopenic group compared with the normal group. Anisotropy of trabecular bone microarchitecture, as measured by the ratios of the mean intercept length (MIL) values (MIL1/MIL3, etc.), and the anisotropy in elastic modulus (E1/E3, etc.), were greater in the osteopenic group compared with the normal group. The correlations between the measures of architecture and moduli are higher than those between elastic moduli and BMD. Stepwise multiple regression analysis showed that while App BV/TV is highly correlated with the mechanical properties, additional structural measures do contribute to the improved prediction of the mechanical measures. This study demonstrates the feasibility and potential of using MR imaging with $\mu$FE modeling in vivo in the study of osteoporosis.

**Keywords:** Magnetic resonance imaging; Mechanical properties; Trabecular bone architecture

*Current address: Synarc, Market Street, San Francisco, California, USA.

*Correspondence and offprint requests to:* Sharmila Majumdar, PhD, Department of Radiology, MRSC, UCSF, 1 Irving Street AC 109, San Francisco, CA 94143-1290, USA. Tel: +1 (415) 476 6830. Fax: +1 (415) 476 8809. e-mail: majumdar@mrsc.ucsf.edu

## Introduction

Bone strength is one of the most important factors in the assessment of fracture risk and efficacy of therapeutic interventions in osteoporosis. The propensity to fracture is determined by both extrinsic factors, such as the force of a fall, and intrinsic factors that define the strength of the bone, including the density of bone, both cortical and trabecular, bone macroarchitecture and geometry, trabecular bone microarchitecture, matrix composition of the bone itself, and rate of turnover. The ultimate aim of therapeutic drugs is to decrease fracture risk by increasing bone strength. In most cases bone mineral density (BMD) is used as a surrogate for fracture risk; however, BMD does not entirely account for fracture risk, or therapeutic effects. Thus, in order to obtain a more complete description of skeletal status, researchers have undertaken the investigation of other factors that potentially affect bone strength. Current in vivo imaging techniques and computerized image processing have made it possible to investigate noninvasively the contribution of trabecular bone microarchitecture to bone mechanical properties, and hence to fracture risk, and to the underlying mechanisms of osteoporosis treatment.

In this paper we present our results determining the effects of trabecular bone microarchitecture on bone mechanical properties using a combination of magnetic resonance (MR) imaging and micro-finite element analysis ($\mu$FE) in the distal radius. We relate these measures to BMD at the distal radius, lumbar spine and proximal femur, as well as to the systemic rate of bone turnover measured using urinary C-telopeptides (CTX) normalized to creatinine, serum CTX and serum osteocalcin (OC). We also determine whether the inclusion of structure measures improves the prediction of bone mechanical properties as assessed using $\mu$FE analysis.

## Materials and Methods

### *Subjects*

Subjects participating in a randomized, double-masked, multicenter study of a selective estrogen receptor modulator, idoxifene, were recruited for this additional ancillary study at two institutions, namely University of California, San Francisco (UCSF) and University of Washington (UW), Seattle, in concordance with the regulations of the Institutional Review Board at the respective institutions.

The subjects were recruited into the study if they were (i) postmenopausal ($\geqslant$12 months but $\leqslant$8 years postmenopausal) and $\leqslant$65 years of age, or (ii) postmenopausal ($\geqslant$12 months postmenopausal) and osteopenic, as defined by the WHO criterion with spine or femur (BMD) $T$-score between $-1$ and $-2.5$.

Subjects with anatomic deformities of the spine sufficient to interfere with the assessment of BMD were excluded. All subjects with fractures in the lumbar (L1–L4) vertebrae were excluded. Subjects were recruited such that they did not have (i) a history of substance abuse (including alcohol) within the past 2 years, (ii) treatment with any investigational drug within the last 30 days, (iii) treatment with any approved or investigational drugs for the prevention or treatment of osteoporosis ($\leqslant$6 months), (iv) other medical conditions and lifestyle habits which would affect bone turnover or (v) chronic use of medications known to affect bone turnover. Although these exclusion criteria control and account for trabecular bone changes for the limited period of a few years, previous history and lifetime impact of such factors on trabecular bone are not accounted for in this study, and may result in some heterogeneity in the sample. In addition, for the MR scans, subjects with pacemakers, metallic fragments in the eyes, vascular clips, aneurysm clips, cochlear implants, claustrophobic subjects and those with a body weight greater than 113 kg were excluded. As the investigational drug required monitoring the uterus and cervix, other exclusion criteria pertaining to uterine health were also included.

A total of 59 subjects were enrolled in this ancillary study, and consisted of (I) postmenopausal women with normal BMD ($n$ = 22, mean age 58 $\pm$ 7 years) and (II) postmenopausal women with BMD $-1$ SD to $-2.5$ SD below young normal ($n$ = 37, mean age 62 $\pm$ 11 years).

### *BMD Measurements*

BMD measurements were obtained using dual-energy X-ray absorptiometry (DXA). The lumbar spine (anterior–posterior projection (AP) L1–L4), distal radius and hip were scanned using Hologic QDR 4500 scanners (Hologic, Waltham, MA). The data were analyzed using the manufacturer's software.

### *Bone Turnover Measurements*

All measurements of bone turnover were made at a central laboratory. A second morning void urine specimen was used for evaluation of urinary type I collagen C-terminal telopeptide (urinary CTX) excretion. Urinary CTX was measured using an enzyme-linked immunoassay (CrossLaps ELISA, Osteometer Biotech, Denmark) and corrected for urinary creatinine concentrations measured by standard colorimetric methods. The premenopausal reference range for this assay is 194 $\pm$ 107 $\mu$g/mmol creatinine [1]. Serum total osteocalcin was measured with an immunoradiometric assay recognizing intact molecule and N-mid fragment (ELISA-OSTEO, Cis BioInternational, France). The premenopausal reference range for this assay is 9.9 $\pm$ 3.1 ng/ml [1]. Serum (CTX) breakdown products were measured by a two-site ELISA (Serum Crosslaps one step, Osteometer Biotech, Denmark). The premenopausal reference range for this assay is 2428 $\pm$1039 pmol/l.

### *MR Imaging*

All MR images were acquired using a General Electric Signa scanner operating at 1.5 T (General Electric Medical Systems, Milwaukee, WI). Images were obtained at the distal radius, using a quadrature wrist coil (GE/Medical Advances ) at UCSF and a custom-built phased-array coil at UW. The patient lay supine with the arm at the side. A coronal, spin-echo localizer was used to identify axial sections starting 14 mm proximal to the joint line and extending into the radial shaft. At these locations axial high-resolution fast gradient echo images were obtained at a spatial resolution of 156 $\mu$m in-plane and 500 $\mu$m in slice direction. The flip angle, echo time and repetition time were 30°, 5.6 ms and 29 ms, respectively. The total imaging time for the high-resolution scan was 12 min.

### *MR Image Analysis*

The MR scans were transferred to an independent Sun Workstation and processed using software developed in-house based on an IDL (Research Systems, Boulder, CO) interface. For the two different coil geometries used in this study different correction algorithms were required to account for coil inhomogeneities. For the quadrature wrist coil used at the UCSF site, a correction algorithm based on a priori phantom scans was used to correct the image inhomogeneity along the longitudinal axis, or along the shaft of the radius [2]. For the phased-array coil used at UW correction maps based on low-pass filtered versions of the actual high-resolution images were used to correct the inhomogeneities due to the coil geometry [3].

An automatic contour tracking algorithm was used to identify the inner rim of cortical shell. An intensity-based criterion utilizing the coronal localizer scan was used for automatic identification of the end plate [4]. Regions of interest (ROI) were selected beginning 14 mm from the end plate, and extending into the radial shaft (Fig. 1). Two-dimensional ROIs defined by the automated identification of the inner cortex were used to determine irregular regions of interest consisting of trabecular bone only, as shown in Fig. 1. In addition, a three-dimensional (3D) rectangular volume of interest (VOI) extending over at least 7.5 mm was determined for 3D analysis of bone structure and for finite element modeling (Fig. 2).

A global threshold criterion based on two reference intensity levels, one for marrow fat ($I_m$) and one for bone ($I_b$), was used to segment the images [5]. The intensity of the cortical bone was used to define the bone reference $I_b$ as follows: Smoothed intensity profiles along rays normal to the cortical bone surface were calculated, and the cortical intensity for each ray was taken as the value of the first minimum outside the trabecular region. The median value from 10 rays was taken as the cortical intensity for a slice. In order to obtain the final mean bone intensity, these intensity values were averaged for

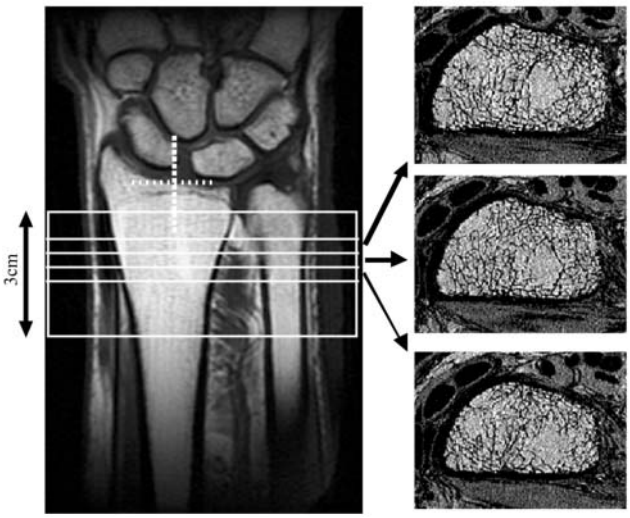


**Fig. 1.** Coronal locator (*left*) and representative slices (*right*) for one patient. The *white box* indicates the 3 cm thick graphic prescription for the high-resolution scan, with the divisions showing the 2.5 mm slabs averaged for analysis. The *dotted cross* indicates the automatically located endplate reference position.

slices more than 2.5 mm from either end of the analysis region in order to avoid regions where the cortex was very thin and could lead to errors in the choice of the bone intensity. The marrow reference intensity $I_m$ was automatically selected using the histogram of intensities within the trabecular bone region as described previously [5]. The global threshold was set using the mean intensity of the trabecular region, $I_{trab}$, to give a bone fraction $BV/TV = (T_{trab} - I_b)/(I_m - I_b)$. This threshold value preserves the average bone fraction for the region in the idealized case where all intensity variations are due to partial volume effects of bone and marrow.

Stereology techniques for quantifying 3D trabecular bone have been implemented in our laboratory [6]. The analysis was conducted over only a trabecular bone region in the radius (Fig. 1). Using the segmented binary image the total number of bone pixels in each ROI and the total area of the ROI were used to compute the App BV/TV. The total number of edges $I_L$ between bone and marrow phases was found by passing a set of rays through the 3D image for each angle pair ($\theta$, $\phi$) (for a 2D analysis, $\phi = 0$). The mean intercept length (MIL) as a function of angle $L(\theta, \phi)$ was then calculated as $2App\ BV/TV \times T_L/I_L$, where $T_L$ is the total length of the lines passing through the image. Using the mean intercept lengths, the components of the 3D fabric tensor, H, were calculated with a least squares fitting technique. The eigenvalues of the fabric tensor were obtained using singular value decomposition. The eigenvectors were ordered such that MIL1 > MIL2 > MIL3 were related to the mean thickness of trabeculae along the principal structural orientations. The largest eigenvalue and its orientation denotes the preferred trabecular orientation magnitude and direction. The other two eigenvalues

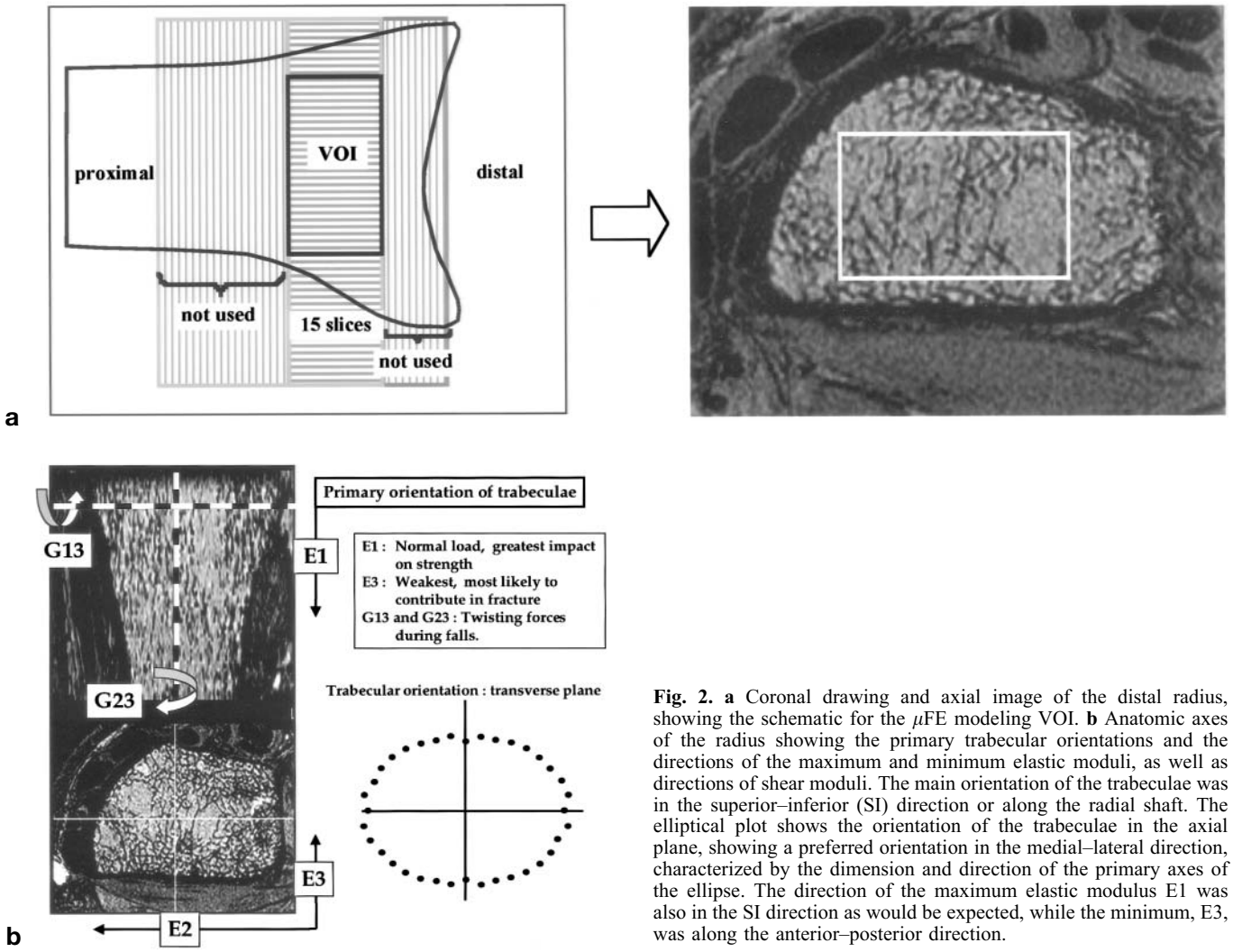


**Fig. 2. a** Coronal drawing and axial image of the distal radius, showing the schematic for the $\mu$FE modeling VOI. **b** Anatomic axes of the radius showing the primary trabecular orientations and the directions of the maximum and minimum elastic moduli, as well as directions of shear moduli. The main orientation of the trabeculae was in the superior–inferior (SI) direction or along the radial shaft. The elliptical plot shows the orientation of the trabeculae in the axial plane, showing a preferred orientation in the medial–lateral direction, characterized by the dimension and direction of the primary axes of the ellipse. The direction of the maximum elastic modulus E1 was also in the SI direction as would be expected, while the minimum, E3, was along the anterior–posterior direction.

provide the other orientations preferred to a lesser extent, and for an isotropic orientation all eigenvalues would be comparable. The structural anisotropy was determined by taking the ratios of the eigenvalues: MIL1/MIL3, MIL2/MIL3 and MIL1/MIL2. Using a slice-by-slice approach other parameters determined were apparent trabecular number, spacing and thickness (App TbN, App TbSp, and App Tb Th).

### *Finite Element Analysis*

The segmented reconstructions of the VOI (Fig. 2a) were converted to $\mu$FE models by converting the voxels (size 156 $\times$ 156 $\times$ 500 $\mu$m) that represent bone tissue to equally shaped 8-node brick elements using a mass-compensated meshing technique [7]. The tissue element properties were chosen to be linear, elastic and isotropic with a Young's modulus of 10 GPa and a Poisson's ratio of 0.3, for all models. Using a special-purpose FE-solver, six FE analyses were performed for each specimen, representing three orthogonal compression tests and three orthogonal shear tests [8]. A homogenization approach was used to calculate the full stiffness matrix for the specimen as a whole from the results of these analyses. An optimization procedure was then used to find a new coordinate system aligned with the best orthotropic symmetry-directions of the specimen. The compliance matrix was rotated to this new orthotropic coordinate system, and the three Young's moduli, three Poisson's ratios and three shear moduli were calculated in these principal directions. The matrices were sorted such that the Young's moduli were in descending order: E1 $\geqslant$ E2 $\geqslant$ E3. The shear moduli were denoted as G12, G23 and G13. The advantage of this optimization and rotation procedure is that the actual values found for the elastic parameters are independent of the rotation of the specimen. The anisotropy ratios E1/E3, E2/E3 and E1/E2 were calculated. An important point to note here is that the slice thickness is greater than the in-plane resolution, and may affect the evaluation of the trabecular anisotropy. To reduce the impact of this anisotropic resolution, the slice direction was selected to be axial, as it is known from histologic studies that the primary orientation in the radius is along the direction of the radial shaft.

*Statistical Analysis*

Descriptive statistics for age, years since menopause, BMD and structure variables were obtained, and minimum, maximum, mean and standard deviations were tabulated. The differences in parameters between subjects with normal BMD and those considered to be osteopenic, based on the lumbar spine or hip BMD, were compared using a *t*-test. For the biomarkers, the *t*-test was done after logarithmic transformation of the data. In addition, the osteopenic subjects were divided into two groups based on their serum CTX values. Since the serum CTX value shows less variability than urinary CTX level, it was assumed to be a more robust identifier of bone resorption. A reference level based on the mean premenopausal level of serum CTX was used to stratify the two groups (i.e., premenopausal value [9] + 1 SD). Subjects who had serum CTX levels greater than the reference level were considered to have high turnover, while those below that level were considered to have low turnover. Differences between each of these groups were determined using a *t*-test. The BMD and biochemical markers were also treated as continuous variables, and the univariate correlation (Spearman rho) between the different parameters was determined. Furthermore, a stepwise multiple regression model was used to determine whether, in addition to the App BV/TV, other measures of bone structure and markers of bone turnover could improve the prediction of the mechanical measures such as the directional elastic moduli, shear moduli and anisotropy of the elastic moduli.

## Results

Baseline demographics, BMD values and bone biochemistry for all of the postmenopausal subjects in this substudy are described in Table 1. The proportion of osteopenic subjects is high (62%), reflecting the inclusion criteria for the study; however, there was no significant difference in age between the two groups.

The mean values for the structural and mechanical measures are listed in Table 2. The trabecular architecture displayed considerable anisotropy, reflecting the orientation of bone strength in response to the predominant loading direction. In the three-dimensional analysis of bone structure we found that the direction of the highest MIL, or the primary trabecular bone direction, was oriented along the superior–inferior (SI or longitudinal) axis, followed by the medial–lateral (ML), and then by the anterior–posterior direction (AP). This is consistent with the fact that the primary loads in

**Table 2.** Range, standard deviation (SD), mean and standard error of the mean (SEM) for trabecular bone structure and mechanical measures over the entire cohort

| | Range (SD) | Mean | SEM |
|---|---|---|---|
| *Trabecular structure measures in the radius* | | | |
| App BV/TV | 0.22–0.45 (0.05) | 0.36 | 0.006 |
| App TbN (1/mm) | 1.12–1.88 (0.16) | 1.68 | 0.021 |
| App TbSp (mm) | 0.30–0.70 (0.08) | 0.39 | 0.010 |
| App TbTh (mm) | 0.18–0.25 (0.02) | 0.21 | 0.003 |
| MIL1 (mm) | 0.36–0.50 (0.03) | 0.44 | 0.004 |
| MIL2 (mm) | 0.25–0.36 (0.02) | 0.30 | 0.003 |
| MIL3 (mm) | 0.21–0.31 (0.02) | 0.26 | 0.003 |
| MIL1/MIL3 | 1.50–1.82 (0.06) | 1.69 | 0.009 |
| MIL2/MIL3 | 1.02–1.26 (0.04) | 1.17 | 0.007 |
| MIL1/MIL2 | 1.36–1.53 (0.05) | 1.44 | 0.005 |
| *Mechanical measures in the radius* | | | |
| E1 (GPa) | 0.20–3.21 (0.59) | 2.05 | 0.080 |
| E2 (GPa) | 0.13–2.00 (0.40) | 1.21 | 0.052 |
| E3 (GPa) | 0.08–1.44 (0.27) | 0.68 | 0.035 |
| G23 (GPa) | 0.07–0.63 (0.13) | 0.33 | 0.017 |
| G13 (GPa) | 0.05–0.77 (0.14) | 0.40 | 0.018 |
| G12 (GPa) | 0.07–0.95 (0.18) | 0.60 | 0.023 |
| E2/E3 | 1.22–2.37 (0.25) | 1.84 | 0.032 |
| E1/E3 | 2.21–4.37 (0.51) | 3.18 | 0.066 |
| E1/E2 | 1.41–2.29 (0.21) | 1.74 | 0.026 |

**Table 1.** Mean, standard deviation (SD) and standard error of the mean (SEM) for patient demographics, bone mineral density and biochemical markers over the entire cohort

| | Normal | | | Osteopenic | | |
|---|---|---|---|---|---|---|
| | Mean | SD | SEM | Mean | SD | SEM |
| *Demographics* | | | | | | |
| Age (years) | 55.8 | 3.94 | 0.78 | 56.4 | 3.95 | 0.61 |
| Years since menopause | 3.4 | 1.93 | 0.37 | 5.9 | 5.51 | 0.84 |
| *Bone mineral density*[a] | | | | | | |
| Distal radius BMD ($gm/cm^2$) | 0.68 | 0.05 | 0.01 | 0.63 | 0.06 | 0.01 |
| Mean BMD (L1–L4) ($gm/cm^2$) | 0.63 | 0.26 | 0.06 | 0.54 | 0.14 | 0.02 |
| Femoral neck BMD ($gm/cm^2$) | 0.77 | 0.06 | 0.01 | 0.70 | 0.07 | 0.01 |
| Total femur BMD ($gm/cm^2$) | 0.91 | 0.07 | 0.01 | 0.82 | 0.07 | 0.01 |
| *Biochemical markers* | | | | | | |
| Urinary CTX/creatinine ($\mu g$/mmol Cr) | 321.56 | 162.70 | 31.31 | 305.23 | 128.80 | 19.64 |
| Serum CTX (pmol/l) | 4818.12 | 1786.06 | 350.27 | 5486.05 | 2762.34 | 421.25 |
| Osteocalcin (OC) (ng/ml) | 29.37 | 9.49 | 1.82 | 31.32 | 9.84 | 1.50 |

[a] By DXA.

**Table 3.** Correlation ($R$) between bone mineral density and biochemical markers

| | Spine BMD | Total hip BMD | Femoral neck BMD | UD radius BMD | Total radius BMD | OC |
|---|---|---|---|---|---|---|
| Spine BMD | 1.000 | | | | | |
| Total hip BMD | 0.387 | 1.000 | | | | |
| Femoral neck BMD | 0.313 | 0.773 | 1.000 | | | |
| UD radius BMD | 0.244 | 0.274 | 0.340 | 1.000 | | |
| Total radius BMD | 0.309 | 0.240 | 0.458 | 0.833 | 1.000 | |
| OC | −0.165 | −0.089 | −0.094 | −0.147 | −0.074 | 1.000 |
| Urinary CTX | −0.022 | 0.107 | 0.126 | −0.094 | 0.044 | 0.678 |

UD, ultradistal; OC, osteocalcin.

**Table 4.** Correlation ($R$) between bone mineral density (UD radius), biochemical markers (OC and Urinary CTX) and measures of trabecular bone structure

| | UD radius | OC | Urinary CTX |
|---|---|---|---|
| App BV/TV | 0.404 | −0.103 | 0.048 |
| App Tb Th | 0.436 | −0.189 | −0.094 |
| App TbN | 0.169 | −0.101 | 0.136 |
| App TbSp | −0.308 | 0.091 | 0.105 |
| MIL3 | 0.435 | −0.289 | −0.222 |
| MIL2 | 0.405 | −0.214 | −0.108 |
| MIL1 | 0.381 | −0.176 | −0.091 |
| MIL 1/3 | −0.241 | 0.297 | 0.174 |
| MIL2/3 | −0.035 | 0.274 | 0.182 |
| MIL1/2 | −0.244 | −0.037 | −0.059 |

UD, ultradistal; OC, osteocalcin.

the radius are directed or applied along the length of the radius (SI axis) (Fig. 2b), consistent with the radiographic appearance.

The data on directional elastic moduli were consistent with the MIL values, where the highest elastic modulus E1 was in the SI direction, the second highest (E2) was in the ML direction, and the lowest (E3) was in the AP direction (Fig. 2b). The differences between the directional elastic moduli were significant ($p<0.0001$). E1 was $\sim$3 times greater than E3, and $\sim$1.8 times greater than E2 as demonstrated by the ratios E1/E3 and E1/E2. Similarly E2 was $\sim$1.7 times greater than E3. These differences are consistent in trend compared with the differences in MIL1, MIL2 and MIL3, but are larger in magnitude. As seen from Table 2, G12 is greater than G23 and G13, which are comparable in magnitude.

The correlations between the biochemical markers and BMD (Table 3) are low, consistent with other published values [9]. The correlations between the structure measures in the radius, biochemical markers and BMD are shown in Table 4. The correlations between the biochemical markers and trabecular bone microarchi-

**Table 5.** Mean $\pm$ SEM of trabecular bone structure and mechanical measures for normal and osteopenic groups, and in the osteopenic category for low- and high-turnover groups

| Parameter | Normal ($n$ = 22) | Osteopenic ($n$ = 37) | Osteopenic low turnover (serum CTX) ($n$ = 10) | Osteopenic high turnover (serum CTX) ($n$= 27) |
|---|---|---|---|---|
| App BV/TV | 0.370 ± 0.010 | 0.354 ± 0.009 | 0.375 ± 0.041 | 0.345 ± 0.054 |
| App TbN | 1.710 ± 0.026 | 1.656 ± 0.028 | 1.692 ± 0.105 | 1.641 ± 0.191 |
| App TbSp | 0.371 ± 0.012 | 0.399 ± 0.014 | 0.373 ± 0.044 | 0.410 ± 0.096 |
| App TbTh | 0.218 ± 0.004 | 0.212 ± 0.003 | 0.221 ± 0.019 | 0.209 ± 0.016 |
| MIL1 | 0.446 ± 0.007 | 0.432 ± 0.005 | 0.441 ± 0.027 | 0.429 ± 0.029 |
| MIL2 | 0.310 ± 0.006 | 0.299 ± 0.004 | 0.308 ± 0.022 | 0.296 ± 0.024 |
| MIL3 | 0.268 ± 0.006 | 0.254 ± 0.003 | 0.264 ± 0.021 | 0.251 ± 0.019 |
| MIL 1/3 | 1.667 ± 0.015 | 1.701 ± 0.007 | 1.677 ± 0.037 | 1.711 ± 0.042 |
| MIL 2/3 | 1.160 ± 0.011 | 1.177 ± 0.007 | 1.168 ± 0.036 | 1.181 ± 0.042 |
| MIL 1/2 | 1.437 ± 0.007 | 1.446 ± 0.007 | 1.436 ± 0.039 | 1.449 ± 0.041 |
| E1 | 2.204 ± 0.118 | 1.972 ± 0.099 | 2.202 ± 0.142 | 1.899 ± 0.633 |
| E2 | 1.287 ± 0.087 | 1.160 ± 0.065 | 1.349 ± 0.096 | 1.098 ± 0.405 |
| E3 | 0.754 ± 0.061 | 0.631 ± 0.040 | 0.769 ± 0.063 | 0.586 ± 0.245 |
| G23 | 0.368 ± 0.028 | 0.316 ± 0.020 | 0.374 ± 0.031 | 0.297 ± 0.121 |
| G13 | 0.439 ± 0.032 | 0.375 ± 0.022 | 0.438 ± 0.034 | 0.354 ± 0.129 |
| G12 | 0.638 ± 0.038 | 0.579 ± 0.029 | 0.663 ± 0.043 | 0.552 ± 0.187 |
| E2/E3 | 1.765 ± 0.055 | 1.879 ± 0.038 | 1.777 ± 0.056 | 1.911 ± 0.243 |
| E1/E3 | 3.104 ± 0.124 | 3.222 ± 0.078 | 2.917 ± 0.116 | 3.332 ± 0.468 |
| E1/E2 | 1.761 ± 0.044 | 1.720 ± 0.034 | 1.644 ± 0.051 | 1.745 ± 0.219 |
| Radius BMD | 0.443 ± 0.12 | 0.407 ± 0.008 | 0.432 ± 0.049 | 0.398 ± 0.049 |

Subjects with serum CTX levels >1 standard deviation above the premenopausal level were considered to be in the high-turnover category.

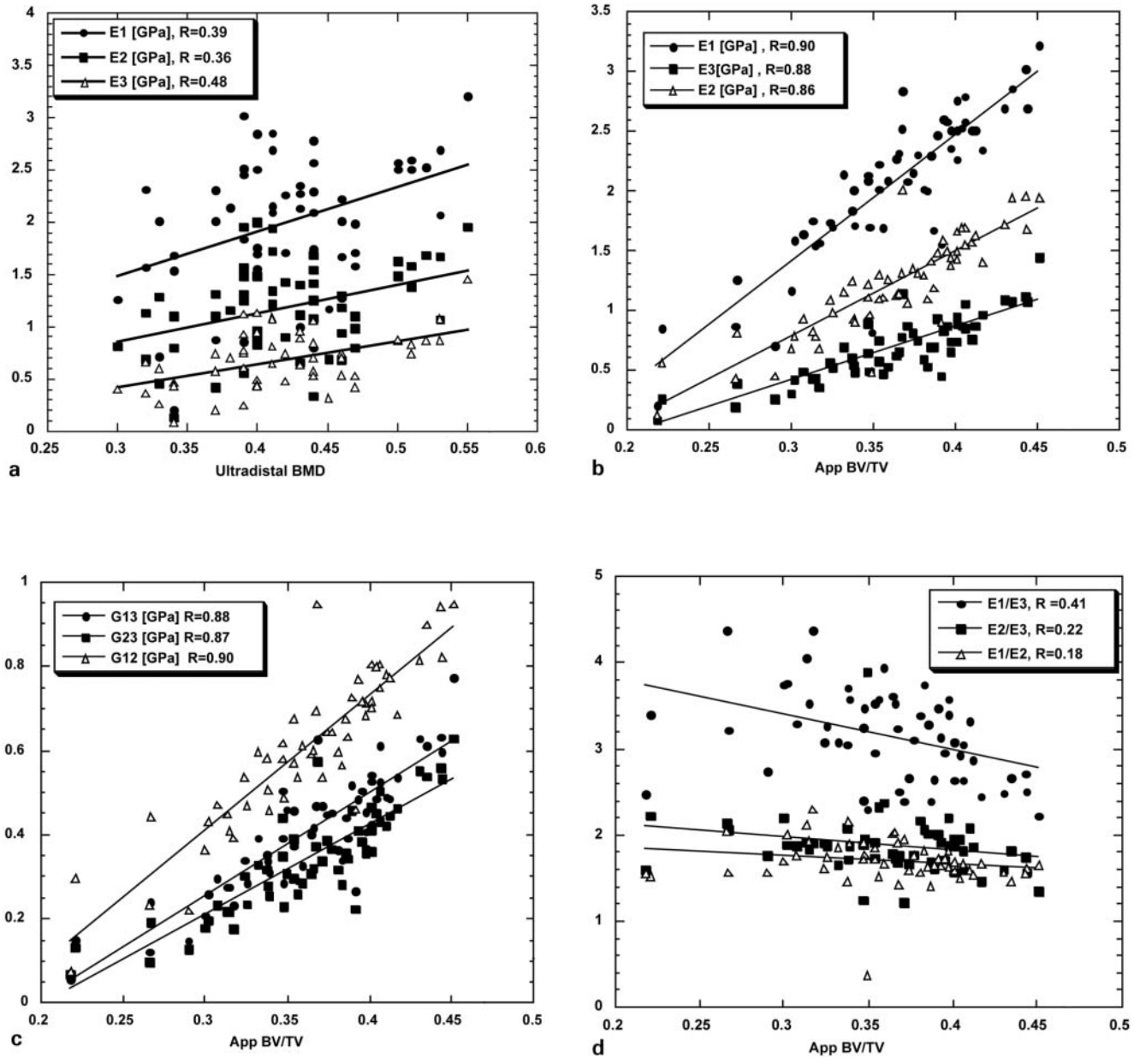


**Fig. 3a-d.** Variation of elastic modulus as a function of **a** BMD and **b** App BV/TV. Variation of shear modulus as a function of **c** App BV/TV. Variation of anisotropy of the elastic modulus as a function of **d** App BV/TV. (*Continued over*)

tecture measures are low, but marginally higher than the correlation between BMD and biochemical markers. The correlations between BMD and measures of trabecular architecture are typically moderate (0.3–0.49), and show that App BV/TV, TbN and TbTh increase, while App TbSp decreases, as the BMD increases.

The variation in the moduli and the measures of anisotropy with App BV/TV and BMD are shown in Fig. 3a–d. The correlations between the measures of architecture and moduli are higher than those between elastic moduli and BMD.

The correlations between E1 and MIL1 and between E2 and MIL2, etc., for all subjects are shown in Fig. 3e–g. The correlation between E1 and MIL1 is lower (0.61) in the osteopenic than the normal group ($R$ = 0.78). Similarly for E2, the correlation with MIL2 was 0.57 for the osteopenic and 0.61 for the normal group, while for E3 versus MIL3 it was 0.66 for the osteopenic and 0.73 for the normal group.

Since the patients were stratified as osteopenic ($n$ = 37) versus normal ($n$ = 22) based on the measures of spine and hip BMD, these measures were significantly different between the two groups. As there was no significant difference in age between these groups, no

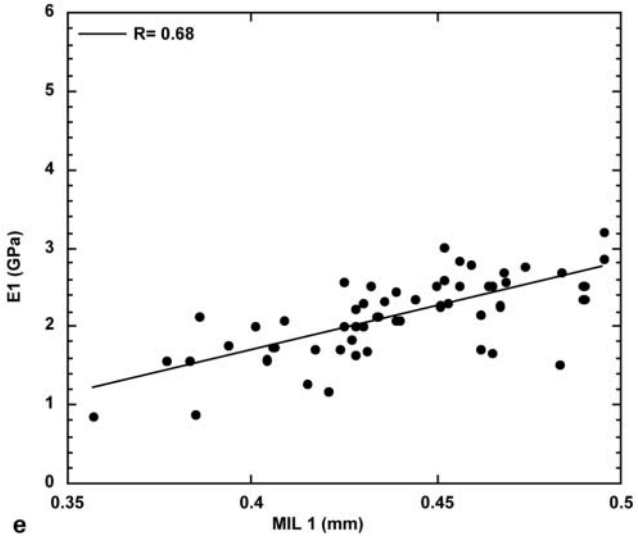


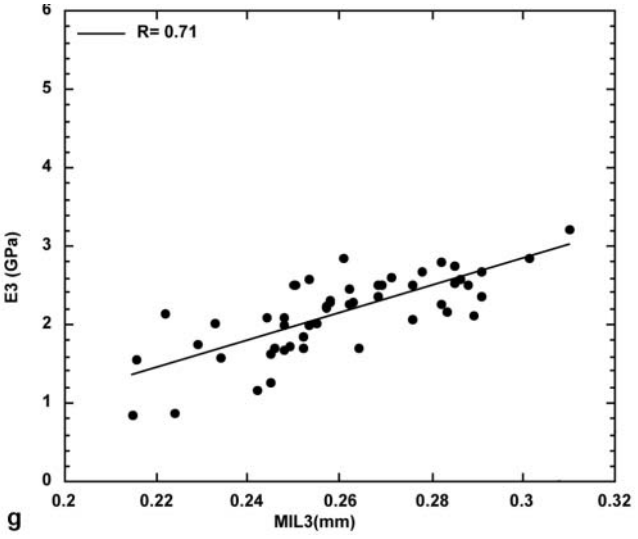


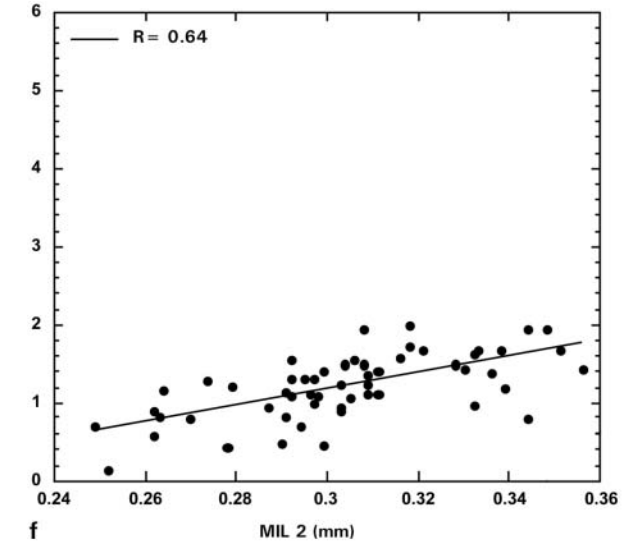


**Fig. 3e–g.** Relationships between **e** MIL1 and E1, **f** MIL2 and E2, and **g** MIL3 and E3.

age adjustment was made. Other measures of BMD such as the ultradistal radial BMD were also lower in the osteopenic group ($p<0.01$). After logarithmic transformation, biochemical markers in the two groups were comparable in value and showed no significant difference between them. App BV/TV, TbTh, TbN were higher, and App TbSp lower, in the normal group compared with the osteopenic group (Table 5). All three directional measures of elastic and shear moduli were lower in the osteopenic group compared with the normal group (Table 5). An interesting finding was that the anisotropy of trabecular bone microarchitecture, as measured by the ratios of the MIL values (MIL1/MIL3, etc.), and the anisotropy in the elastic modulus (E1/E3, etc.), were greater in the osteopenic group than the normal group. The percentage difference, calculated as the difference between the control and osteopenic groups, normalized to the control group, for all parameters is shown in Fig. 4a. Using a one-tailed *t*-test, in addition to the ultradistal BMD measure, the trends in differences in trabecular bone structure and mechanical measures were significant ($p<0.05$) for MIL3, MIL2, MIL1, MIL1/MIL3, E3, G13 and E2/E3 (shown with an asterisk in Fig. 4a).

The structural measures and mechanical measures in the high-turnover and low-turnover groups are shown in Table 5. As can be seen from the table, the osteopenic subgroup with the higher turnover rates had the lowest BMD, App BV/TV, App TbN, TbTh, MIL, elastic moduli and shear moduli values, and the highest App TbSp, and structural and mechanical anisotropy. The percentage difference, calculated as the difference between the low- and high-turnover groups, normalized to the low-turnover group, for all parameters is shown in Fig. 4b. Comparing the two groups, significant differences were seen between E1/E3 and MIL1/MIL3. Interestingly, the anisotropy increases as the App BV/TV decreases (Fig. 3), which is consistent with the differences seen in MIL1/MIL3, etc., and the E1/E3 ratios between normal and osteopenic subjects. It must be kept in mind that the number of subjects per group becomes smaller with these further subdivisions. Thus these results merely support the hypothesis that even in the BMD-based subdivisions of normal and osteopenic groups, levels of resorption are significantly varied and may affect the trabecular structure and mechanical properties.

Table 6 shows the results of multiple regression analysis, which was directed to examine whether a combination of ultradistal BMD, biomarkers and measures of bone structure (in addition to App BV/TV) would improve the prediction of mechanical properties. The results indicate that while App BV/TV is highly correlated with the mechanical properties, additional structural measures do contribute to the improved prediction of the mechanical measures. For improvement in the prediction of the elastic and shear moduli, typically App TbN (which is independently determined from App BV/TV) played a role, and App TbSp, although indirectly determined from App BV/TV and App TbN, also played a role. In the improved

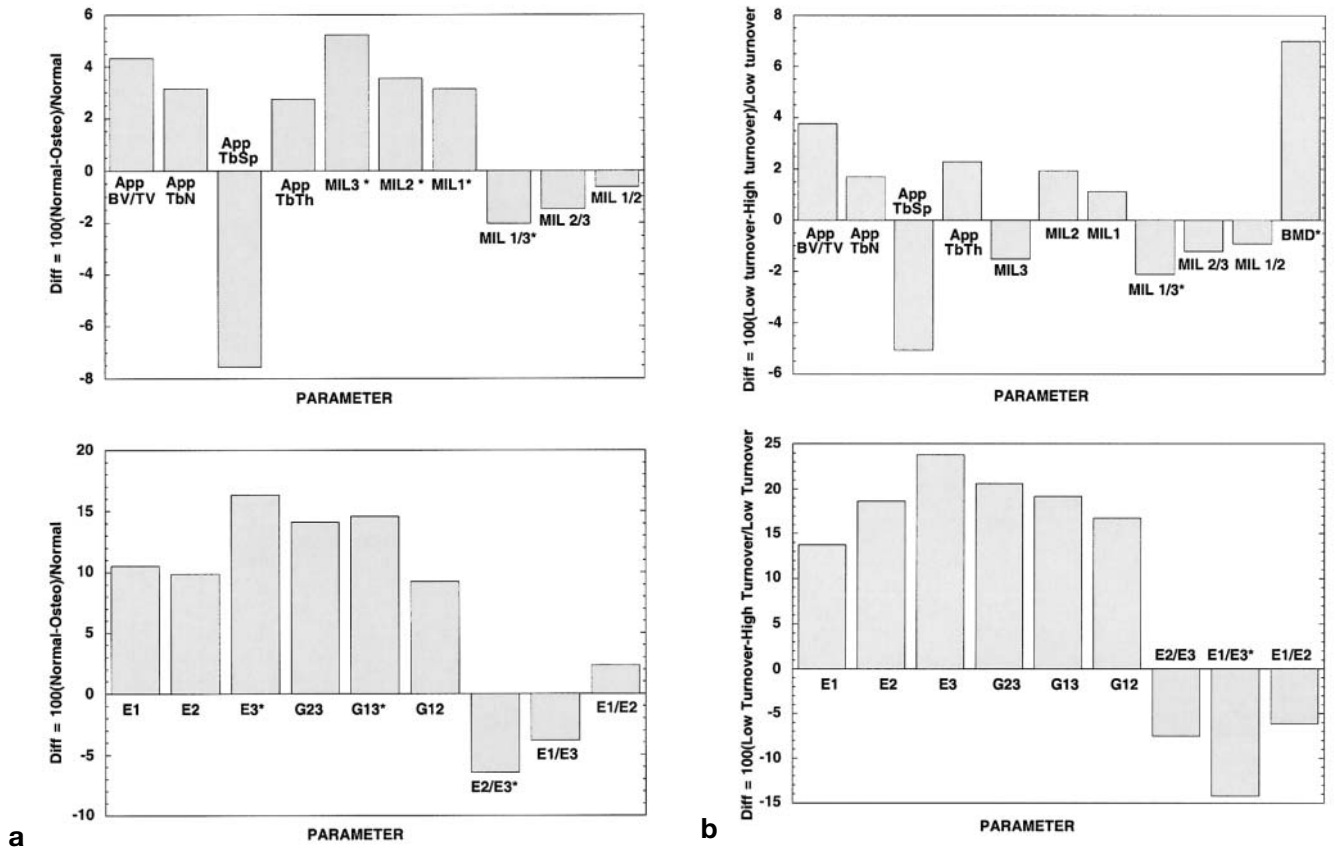


**Fig. 4. a** A plot of the percentage difference in the measures of BMD, structure and mechanical properties between the normal and osteopenic subject groups. *$p$<0.05 between groups. **b** A plot of the percentage difference in the measures of BMD, structure and mechanical properties in the osteopenic subjects subdivided into two groups based on the levels of serum CTX. The group shown as low turnover in the figure had serum CTX levels <+1 SD of premenopausal mean, while the high-turnover group had serum CTX levels >+1 SD of premenopausal mean. *$p$<0.05 between groups.

prediction of mechanical anisotropy, i.e., E1/E3 and E2/E3 and E1/E2, the ratios MIL1/MIL3 played a role as would be expected. The measures of biomechanical properties, such as E2, where the additional measures did not contribute to their improved prediction are not shown in Table 6.

**Table 6.** Results from a stepwise regression model showing the increase in the adjusted $R^2$ when other parameters in addition to App BV/TV were included in the model

| | $R^2$ (with App BV/TV) to Adj $R^2$ | Significant contributions from | Significance level $p$< |
|---|---|---|---|
| E1 | 0.80 to 0.83 | App TbN | 0.02 |
| | | MIL2/3 | 0.03 |
| E3 | 0.74 to 0.81 | App TbSp | 0.02 |
| | | MIL1/MIL3 | 0.14 |
| E1/E3 | 0.19 to 0.69 | App TbSp | 0.0005 |
| | | MIL2/MIL3 | 0.001 |
| | | App TbTh | 0.01 |
| | | App TbN | 0.02 |
| E2/E3 | 0.10 to 0.59 | App TbTh | 0.002 |
| | | MIL2/MIL3 | 0.09 |
| E1/E2 | 0.07 to 0.55 | App TbSp | 0.00 |
| | | Radius BMD | 0.02 |
| | | MIL1/MIL2 | 0.07 |
| G23 | 0.75 to 0.80 | App TbSp | 0.03 |
| | | MIL1/MIL3 | 0.007 |
| G13 | 0.77 to 0.84 | App TbSp | 0.10 |
| | | MIL2/MIL3 | 0.09 |

The significance level $p$ is given for each variable.

## Discussion

In previous studies we have demonstrated differences in radial bone structure with age, osteoporotic status and the presence of hip fractures using high-resolution MR images in the distal radius, and our current results pertaining to the correlation between structural measures and BMD are consistent with these previous studies [5,10]. Additionally, in this paper we have used these in vivo images not only for the computation of trabecular bone microarchitecture measures but also in $\mu$FE models to calculate the mechanical properties of trabecular bone.

The directional mechanics of bone may potentially play an important role in predicting biomechanics, as has been shown in vitro [6,11,12], and hence these properties and their relative changes may be useful for fracture prediction and assessing response to therapy. In this study, using a stepwise multiple regression model, we found that App BV/TV clearly explained 73–83% of the variation in elastic moduli and shear moduli, but other measures of bone structure such as App TbSp and TbN increased the adjusted correlation coefficient with the mechanical measures. The measures of mechanical anisotropy and the shear moduli showed that the structural anisotropy measures such as MIL1/MIL3 improved the adjusted correlation coefficient significantly. These results in vivo are consistent with results seen in vitro by Ulrich et al. [11] and Kabel et al. [12]. Using higher-resolution $\mu$CT images of specimens of trabecular bone, both groups of investigators found improvements in the finite element derived mechanical properties with the inclusion of structural measures.

It should be noted that MR-derived measures of structure, because of the resolution of the images being comparable to the trabecular dimensions, are prone to partial volume effects. With the current methods for choosing the bone/marrow binarization threshold, this implies that measures of App BV/TV, TbN and TbTh are overestimated, while TbSp is underestimated, when compared with significantly higher resolution ($\sim$20 $\mu$m) images in which these parameters are affected to a much lesser extent [13]. For the overestimation of TbN there are at least two possible explanations. The first is that variations in bone marrow intensity are classified as trabeculae depending on the partial volume effect and thresholding criteria. The second is that due to reduced resolution and partial volume effects, curved and longer trabeculae may be broken into multiple components, resulting in a higher apparent TbN. Both these effects may be present, and would in turn contribute to the measures of trabecular structure anisotropy (e.g., the MIL ratios such as MIL1/MIL3). Though the magnitude of the measures differs, it has been shown that these measures of trabecular bone structure derived from MR images are highly correlated with those obtained from higher-resolution images (obtained from three-dimensional reconstructions from serial grinding sections) [13] and also predict the mechanical properties in vitro [6]. Similarly, $\mu$FE element models based on MR images provide measures of Young's moduli, shear moduli and elastic anisotropy that are highly correlated but not identical in absolute value to those obtained from $\mu$FE analysis of higher-resolution $\mu$CT [14] images. The lower values of elastic modulus such as E3, and the anisotropy ratios E1/E3 that depend significantly on the contribution of the thinner trabeculae which may be unresolved in the MR images, show in general poorer correlation. These resolution-dependent effects must be noted when examining the data and determining the statistical contributions of parameters such as MIL3, E3 and the anisotropy ratios involving these measures. The higher the spatial resolution, clearly the lower the partial volume effects would be in the images; however, higher spatial resolution would actually decrease the relative signal-to-noise ratio of the images. Hence, at some point, there will be a trade-off between the reduction in partial volume effects and the concomitant increase in noise in the image. Our spatial resolution is anisotropic, with the resolution being a factor of 3 lower in the slice direction. This in fact could lead to an artifactual definition of the primary orientation of the trabeculae and the direction of greatest elastic modulus. However, in the distal radius the primary orientation of the trabeculae is known from previous studies [15] to be superior–inferior, along the shaft, and hence we selected our slice direction so as to reduce the impact of our anisotropic resolution on the structure and mechanical measures.

Another point to note is that the structural measures were obtained over an irregularly shaped volume, whereas the finite element model was obtained for a regular rectangularly shaped volume of interest. The trabecular bone analysis region was selected to maximize the trabecular bone sampled, while the finite element analysis was done in a regular region to contain the complexity of the analysis and ensure reasonable computation times. Despite this the correlation between elastic measures and structure measures is high.

We find that the differences between the normal and osteopenic subjects are greater in the direction of the weaker modulus, while the structural and mechanical anisotropy is higher in the group of osteopenic subjects. In addition the correlation is weaker between the elastic modulus and the MIL measures in the osteopenic group. These results imply that in osteopenics, in the radius, the thinner trabeculae are lost first, which is consistent with results in the spine, where Mosekilde showed that horizontal thinner trabeculae are lost first with aging and osteoporosis [16]. Similarly, measures of anisotropy were greater in the group with bone turnover rates greater than the premenopausal level +1 SD, compared with the group of subjects with bone resorption rates below this cut-off. This is consistent with the concept that increases in resorption lead to a loss of trabeculae, with a greater loss in the direction of the thinner trabeculae resulting in an increase in anisotropy. However, it must be noted that the subgroups had in some cases a small sample size, and the numbers in each group were not equal. Garnero et al. [9], in a larger

cohort, used the cut-off for high resorption rate to be the premenopausal level +2 SD; however, given our small sample size, and the range of resorption rates, this subdivision of the groups was not possible. Thus, in this sort of group-based analysis, the trends are interesting, and while some of these results showed significance these require further validation in a larger sample size. It must also be noted that serum and urinary biomarkers in large clinical trials and epidemiologic studies show large variations between and within individuals, and while in this study with a small number of subjects we did not expect to find significance between the two groups, the trends seen are potentially exciting. An extension of this study would be one mapping the longitudinal changes in these markers, and their impact on structure and biomechanics. While these studies have been initiated, they are not completed, and will be reported at a later date.

Garnero et al. [9] presented baseline data on 305 postmenopausal women in the OFELY study, showing very similar values for ultradistal BMD, urinary CTX and serum OC. The correlation coefficient between BMD and these biomarkers was low in that study, and consistent with our findings in the current study. BMD is frequently used as one of the parameters for stratifying patients, and it is often used as a gold standard or comparison metric, but it must be noted that BMD measures are a measure of projected density, while structure and mechanical measures represent three-dimensional properties of trabecular bone. This is demonstrated in the mediocre correlation between BMD and the measures of bone structure and between BMD and the mechanical parameters. While, because of our small sample size, we cannot draw any conclusions, we do find the correlation between biomarkers and architecture to be marginally better than that between BMD and biomarkers, perhaps implying that bone turnover affects the architecture, and these changes in cross-sectional measures may not be resolved by projectional DXA measures.

Thus far we have selected a single region of interest in the distal radius and looked at the structural and mechanical variations in bone structure over that region. The variation in bone structure as a function of increasing distance from the joint line and epiphyseal plate, relative to the total radial length, has not been studied. There is clearly a vast amount of further regional analysis that potentially awaits investigation, and could enhance our understanding of the complex interactions between the onset of osteoporosis at a systemic (or at least a spinal or femoral) level, biochemical markers, and structure and mechanical properties of the appendicular skeleton.

One of the factors affecting the evaluation of trabecular bone structure and related mechanical parameters relies on the segmentation or definition of the trabecular bone fraction. In the limited resolution of in vivo MR images, partial volume effects are inevitable. To segment such images into bone and marrow phases implies standardization of a procedure; however, no preferred procedure has been established yet. Ouyang et al. [17] used a calibration technique in calcaneus images with poorer resolution, where regions of interest in cortical bone, tendon and air were used to derived a ''bone intensity'', and subcutaneous fat and marrow fat were used to define a ''fat intensity''. This technique was not appropriate, as in the distal radius the marrow spaces are very small, unlike the ''pseudo-tumor'' region in the calcaneus, and the subcutaneous fat layer is excessively thin, and reproducibility of such a segmentation procedure was very poor. Instead we adopted a histogram-based definition of the marrow intensity region, where the peak of the histogram was used as a reference, and the relative decrease in histogram height to half its full height was used to define the marrow intensity [5]. The reproducibility of this procedure ranged from 2% to 4% [4]. However, another approach, based on a probabilistic assignment of pixels to bone and marrow developed by Hwang et al. [18] and utilized in recent studies [19] also represents a potentially promising way of segmenting such images. These techniques have not yet been evaluated, although studies have been proposed, and will be reported on in the future.

In this study we have restricted the measures of trabecular structure to mean intercept length based techniques. Clearly further analysis using emerging techniques for characterizing trabecular bone architecture such as the direct measures [20], assessment of tubularity [19,21], and directional assessments of trabecular thickness, spacing and number distributions [22], may potentially be very useful in furthering our understanding of the interrelationships between bone structure, mechanical properties, turnover and osteoporotic classifications.

The patients in this study were derived from a continuing study with rigid inclusion criteria, and hence the range of bone mineral densities is limited. Further, we do not include premenopausal or elderly osteoporotic subjects. Also, the distribution of the years since menopause is non-normal and skewed towards the first 5 years. Thus it is evident that the relationships derived between the postmenopausal changes, rates of bone turnover and structure over all possible ranges cannot be derived from this study. However, despite these limitations of the study population, the results are encouraging, validate existing notions with regards to osteoporotic bone loss derived from histomorphometry studies, and clearly indicate the need for a similar evaluation in a diverse and larger cohort. Studies investigating the correlations between measures of structure, bone turnover, and mechanical properties of bone structure, have the potential for elucidating the mechanisms underlying various therapeutic interventions such as selective estrogen receptor modulators or calcitonin. They may provide a partial description for the role of bone quality not only in fracture risk prediction, but also in understanding the pathogenesis of osteoporosis and therapeutic efficacy.

## References


1. Garnero P, Sornay-Rendu E, Chapuy MC, Delmas PD. Increased bone turnover in late postmenopausal women is a major determinant of osteoporosis. J Bone Miner Res 1996;11:337–49.
2. Newitt DC, Majumdar S. Correction for receiver coil inhomogeneity profiles for quantitative analysis of trabecular bone structure from high resolution MRI. Proceedings of the 7th Annual Meeting of the ISMRM 1999, Philadelphia, PA: 1046.
3. Wald LL, Carvajal L, Moyher SE, et al. Phased array detectors and an automated intensity-correction algorithm for high-resolution MR imaging of the human brain. Magn Reson Med 1995;34:433–9.
4. Newitt D, Majumdar S. A semi-automated system for segmenting, registering, thresholding, and analyzing high resolution MRI of trabecular bone. Proceedings of the 8th Annual Meeting of the ISMRM 2000, Denver, Colorado: 127.
5. Majumdar S, Genant HK, Grampp S, et al. Correlation of trabecular bone structure with age, bone mineral density, and osteoporotic status: in vivo studies in the distal radius using high resolution magnetic resonance imaging. J Bone Miner Res 1997;12:111–8.
6. Majumdar S, Kothari M, Augat P, et al. High-resolution magnetic resonance imaging: three-dimensional trabecular bone architecture and biomechanical properties. Bone 1998;22:445–54.
7. Ulrich D, Rietbergen Bv, Weinans H, Ruegsegger P. Finite element analysis of trabecular bone structure: a comparison of image based meshing techniques. J Biomech 1998;31:1187–92.
8. van Rietbergen B, Odgaard A, Kabel J, Huiskes R. Direct mechanics assessment of elastic symmetries and properties of trabecular bone architecture. J Biomech 1996;29:1653–7.
9. Garnero P, Sornay-Rendu E, Duboeuf F, Delmas PD. Markers of bone turnover predict postmenopausal forearm bone loss over 4 years: the OFELY study. J Bone Miner Res 1999;14:1614–21.
10. Majumdar S, Link TM, Augat P, et al. Trabecular bone architecture in the distal radius using magnetic resonance imaging in subjects with fractures of the proximal femur. Magnetic Resonance Science Center and Osteoporosis and Arthritis Research Group. Osteoporos Int 1999;10:231–9.
11. Ulrich D, van Rietbergen B, Laib A, Rüegsegger P. The ability of three-dimensional structural indices to reflect mechanical aspects of trabecular bone. Bone 1999;25:55–60.
12. Kabel J, Rietbergen Bv, Odgaard A, Huiskes R. Constitutive relationships of fabric, density, and elastic properties in cancellous bone architecture. Bone 1999;25:481–6.
13. Kothari M, Chen T, Lin J, Newitt D, Majumdar S, Genant H. Three dimensional bone architecture assessment: impact of image resolution. Osteoporos Int 1997;7:289.
14. van Rietbergen B, Majumdar S, Pistoia W, et al. Assessment of cancellous bone mechanical properties from micro-FE models based on micro-CT, pQCT and MR images. Technol Health Care 1998;6:413–20.
15. Schlenker RA, Von Seggen WW. The distribution of cortical and trabecular bone mass along the lengths of the radius and ulna and the implications for in vivo bone mass measurements. Calcif Tissue Res 1976;20:41–52.
16. Mosekilde L. Sex differences in age-related loss of vertebral trabecular bone mass and structure: biomechanical consequences. Bone 1989;10:425–32.
17. Ouyang X, Selby K, Lang P, et al. High resolution MR imaging of the calcaneus: age-related changes in trabecular structure and comparison with DXA measurements. Calcif Tissue Int 1997;60:139–47.
18. Hwang S, Wehrli F, Williams J. Probability-based structural parameters from three-dimensional nuclear magnetic resonance images as predictors of trabecular bone strength. Med Phys 1997;24:1255–61.
19. Wehrli FW, Hwang SN, Ma J, Song HK, Ford JC, Haddad JG. Cancellous bone volume and structure in the forearm: noninvasive assessment with MR microimaging and image processing [published erratum appears in Radiology 1998;207:833]. Radiology 1998;206:347–57.
20. Hildebrand T, Laib A, Müller R, Dequeker J, Rüegsegger P. Direct three-dimensional morphometric analysis of human cancellous bone: microstructural data from spine, femur, iliac crest, and calcaneus. J Bone Miner Res 1999;14:1167–74.
21. Wehrli FW, Hwang SN, Song HK. New architectural parameters derived from micro-MRI for the prediction of trabecular bone strength. Technol Health Care 1998;6:307–20.
22. Kothari M, Keaveny TM, Lin JC, Newitt DC, Majumdar S. Measurement of intraspecimen variations in vertebral cancellous bone architecture. Bone 1999;25:245–50.


*Received for publication 13 December 2000*
*Accepted in revised form 30 May 2001*